**TECHNICAL ARTICLE—PEER-REVIEWED**

# Fault Feature Extraction of Rolling Element Bearing under Complex Transmission Path Based on Multiband Signals Cross-Correlation Spectrum

Danchen Zhu · Yangyang Pan · Weipeng Gao

**Abstract** Aiming at the problem that bearing fault signals are influenced by complex transmission path and multiple structures of equipment, which results in strong interference components, a fault feature extraction approach for rolling element bearing based on multiband signals cross-correlation spectrum was proposed. First, the improved trend-line method was utilized to improve the calculation efficiency and the influence of the transmission path was removed. Second, the optimal and suboptimal analysis frequency bands were selected with the maximum energy ratio of the feature components as the objective function, which further suppresses the interference of irrelevant components and avoids the blindness selection of the analysis band. Finally, with the advantage of the cross-correlation spectrum, the optimal band signals were combined for analysis to enhance the fault signatures. The simulation signal and the measured bearing inner race and outer race defect signals were utilized for verification; with the help of comparisons, the results indicate that the method in this paper can effectively remove the influence of complex transmission path and accurately extract the bearing fault features from the strong background interference.

## Introduction

Rolling element bearing (REB) is a common component which has been widely used due to its superior performance. However, as REBs usually work in harsh environment, such as high speed and high pressure, the probability of their faults is high, which seriously threatens the safe and stable operation of the whole equipment. As a result, the research on condition monitoring and fault diagnosis of REB has a strong practical significance, which has received extensive attention. Based on the existence studies, vibration-based fault diagnosis is one of the most effective methods, and its focus is on the following aspects:

(1) The problem of selecting effective measurement points, especially the existence of complex transmission path.

(2) How to suppress the interference of irrelevant components and extract the fault features effectively based on the characteristics of bearing fault signals.

(3) The optimization of existing feature extraction methods to guarantee the effectiveness and efficiency of calculation.

To address the above problems, many studies have been carried out. The most classic is the resonant demodulation technique, which is widely applied in engineering practice. However, the central frequency and bandwidth for band-pass filter need to be determined in advance, which greatly limits the application of the method, especially when the

D. Zhu (✉)
Naval Petty Officer Academy, Bengbu, China
e-mail: bryantzdc@sina.com

Y. Pan
First Military Delegate Office of Shanghai under Naval Equipment Department, Shanghai, China

W. Gao
Naval research institute, Beijing, China

signal is polluted by strong background noise. The Fast kurtogram method proposed by Antoni [1] is employed to solve this problem, which improves the effectiveness of fault feature extraction by determining the location of the optimal frequency band through a fixed band division and selection rule. However, the method is also limited by the characteristic of the kurtosis index and the fixed band division technique. To further improve the analysis effect, many researches have been carried out, such as the adaptive correlated kurtogram2, the Fast Fntrogram3, the Enfigram [4], the subband average kurtogram [5], and the Harmogram [6]. The optimization of these algorithms has improved the accuracy of resonant band selection which is more resistance to noise interference. What is more, the empirical wavelet decomposition method proposed in recent years is also usually employed for resonant band selection [7, 8]. But for conditions with strong background noise, it is very difficult to achieve ideal results only by using the optimal band selection approach.

Considering that the components of bearing fault signals are complex, the signal decomposition techniques are employed. They can decompose the signal adaptively into mode functions which contain different frequency components according to the characteristics of the signal, and the fault signatures can be enhanced by selecting the effective components and discarding the irrelevant ones. The most classical method is the empirical mode decomposition (EMD) method [9]; however, the EMD suffers from end effects and mode aliasing. The propose of ensemble empirical mode decomposition approach (EEMD) [10] solves the mode aliasing which exists in the EMD method, but the size of the added white noise and the number of ensembles are still hard to decide; moreover, the analysis efficiency of the method is reduced. To solve the above problems, many improvement methods have been proposed which can achieve ideal results [11–13]. The construction of variational mode decomposition (VMD) method abandons the recursive decomposition pattern in EMD and EEMD [14], which has been widely used in fault diagnosis of REB. However, its decomposition effect is influenced by the number of decomposition level K and the penalty term α. Therefore, numerous studies have be conducted on the two aspects: One is the optimization of the decomposition process of VMD [15, 16], and the other is the optimization of decomposition parameters [17–19]. Based on these two improvements, the effectiveness of the VMD approach can be further guaranteed. What is more, the local mean decomposition (LMD) technique [20] and the singular value decomposition technique [21, 22] are also be widely employed and play an important role in bearing fault detection.

The blind deconvolution approach has gained great attention which aims to solve the problem of complex transmission path. They are used to extract the signal with more obvious fault features, and the influence of transmission path can be eliminated. Commonly used blind deconvolution algorithms include the minimum entropy deconvolution (MED) [23], the maximum correlated kurtosis deconvolution (MCKD) [24], the multipoint optimal minimum entropy deconvolution adjusted (MOMEDA) [25, 26], and the maximum second-order cyclostationarity blind deconvolution (CYCBD) [27]. However, limited by the whole calculation process, the blind deconvolution algorithm is also affected by many parameters, such as the shift number M in the MCKD, the construction of inverse filter, and the determination of filter length. To address these problems, many studies have been carried out, the drawback of parameters selection rely on human experience is solved, and the analysis effect of these approaches is improved [28–31]. The blind deconvolution methods focus on the effect of the transmission path, but it is still essential to further consider how to suppress the influence of complex transmission path more effectively.

Therefore, based on the above description, a fault diagnosis method for REB under complex transmission path based on multiband signals cross-correlation spectrum is proposed in this paper. First, the signal distortion and interference components enhancement caused by the complex transmission path are suppressed by using the trend-line based analysis and spectrum editing method. Second, to eliminate the original noise components caused by the multiple vibration sources of the equipment, the optimal and suboptimal analysis frequency bands are determined by using the maximum energy ratio of the fault features as the target. Finally, fault features in the signal are highlighted with the help of cross-correlation spectrum, and the fault type of REB is accurately judged. The main contributions of this paper are described as follows:

(1) The trend-line-based transmission path elimination technique is improved; the calculation accuracy is ensured, and the efficiency is improved.
(2) The optimal and suboptimal analysis frequency bands are determined based on the principle of maximum fault features ratio, which further suppresses the interference of irrelevant components.
(3) Multiband signals are employed to make full use of the fault features in different frequency bands.
(4) The cross-correlation analysis is utilized to further suppress the random noise components and extract the fault features of REB effectively.

The remainder of this paper is organized as follows. "Spectrum editing" section presents the basic principles of all the techniques employed in this paper, including the improved transmission path elimination method, the optimal analysis frequency band selection approach, and the

1166

J Fail. Anal. and Preven. (2022) 22:1164–1179

cross-correlation analysis. The calculation process of the method is summarized in "The whole structure of the proposed method" section. The simulation and measured signals are adopted to verify the effectiveness of the method in "Simulated verification and Experimental signal verification" sections, respectively. "Conclusion" section draws the conclusions.

## The Basic Principles

### Improved Trend-Line-Based Transmission Path Elimination Method

Based on the results in Ref. [32], for a vibration system, if the excitation signal is white noise, the trend in the amplitude spectrum of response signal can reflect the trend of the transfer function. Hence, by extracting the trend line, the amplitude spectrum of the transfer function for the whole system can be approximated simulated.

Many approaches can extract the trend in the time series, such as the EMD, the wavelet decomposition, the cubical smoothing algorithm with five-point approximation, and seven-point approximation. The implementation of the first two methods is hard and less adaptable, while the last two methods are easy to implement, but when the signal components are complex or the sampling frequency is large, the extracted trends may not ideal, and it needs to try numerous times to obtain better analysis results. What is more, although the beads algorithm can achieve good results, the calculation process requires more parameters to be predetermined which result in high uncertainty.

As a result, to solve the above problems, some improvements have been made as follows:

The logarithmic amplitude spectrum of the signal is not calculated, and the trend line is extracted directly in the amplitude spectrum which is more convenient.

A simpler approach called Savitzky-Golay filtering method (S–G filtering) is employed, and the trend lines are extracted by means of signal fitting with less parameters to be determined.

### S–G Filtering

S–G filtering is performed by the moving window using the least square fitting. Suppose a time series $x(n)$, any point $x(i)$ and $m$ points on both two sides around $x(i)$ are the analysis window; hence, length of the window is $2m + 1$ and the location of $x(i)$ is the center of the window. A $p$-order polynomial $y(n)$ is constructed subsequently to fit the data, which can be expressed as:

$$y(n) = \sum_{k=0}^{p} a_k n^k \qquad \text{(Eq 1)}$$

where $n$ is between $-m$ and $m$, $n \leq 2m + 1$. Then the function is established:

$$F = \sum_{n=-m}^{m} [y(n) - x(n)] = \sum_{n=-m}^{m} \left[ \sum_{k=0}^{p} a_k n^k - x(n) \right] \qquad \text{(Eq 2)}$$

when the minimum value of Eq. 2 is obtained, the fit is better. The above process reveals that the length of the window and the polynomial order have a great influence on the result. When the polynomial order increases, the length of the window is also required to increase to achieve the same smoothing effect, which reduces the calculation efficiency. Therefore, in this paper, the order of polynomial is set to 3 and the window length is chosen ranges from 400 to 600 (odd number) to extract the trend in the time series.

## Spectrum Editing

Spectrum analysis is widely used as an important signal processing method, which is generally obtained by performing the Fourier transform on the signal, including the amplitude spectrum and the phase spectrum. For harmonic signals, their amplitude spectrum is exhibited as a single spectral line, and the amplitude of the corresponding spectral line represents the amplitude of the harmonic signal.

To reduce the effect of harmonic signals, the corresponding spectral lines in the amplitude spectrum can be edited. Like cepstrum analysis, setting the spectral line to zero is the simplest method of spectrum editing, but as there are still components such as white noise in the signal, a simple zeroing may interfere other useful components of the original signal. Therefore, in this paper, spectrum editing is achieved by setting the spectral line's amplitude to a value little higher than the surrounding background noise's amplitudes. By this method, the harmonic interference components are suppressed without affecting other useful components as much as possible. Spectrum editing can be realized as the following steps.

(1) The Fourier transform is employed to the original signal, and the amplitude spectrum and the phase spectrum are acquired.
(2) The amplitude spectrum is edited; the spectral lines' amplitudes corresponding to the harmonic components are suppressed to values slightly higher than the surrounding background noise (the average of the surrounding spectral lines' amplitudes except for the harmonic components' amplitudes).
(3) The edited amplitude spectrum is combined with the original phase spectrum; the inverse Fourier

J Fail. Anal. and Preven. (2022) 22:1164–1179

1167

transform is then utilized to obtain the edited time domain signal.

## The Transmission Path Elimination Technique

In time domain, supposing an excitation signal x(t), the unit impulse response of the transfer function is h(t), and the response signal y(t) can be expressed by a convolution process as:

$$y(t) = x(t) * h(t) \qquad \text{(Eq 3)}$$

where * denotes the convolution operator. Then in the frequency domain, x(t), h(t) and y(t) can be transformed into the amplitude spectrum $X(\omega)$, $H(\omega)$ and $Y(\omega)$ using the Fourier transform. Hence, the relationship among them is also changed and can be expressed as:

$$Y(\omega) = X(\omega)H(\omega) \qquad \text{(Eq 4)}$$

Equation 4 shows that the amplitude spectrum of the response signal is the product of the amplitude spectrum of the excitation signal and the amplitude spectrum of the transfer function. Since the original bearing vibration signal generated during the rotating of REB will transmit through complex transmission path before being collected, the amplitude spectrum of measured bearing vibration signal is also the product of the amplitude spectrum of the internal fault excitation signal and the amplitude spectrum of the complex transfer function. If the amplitude spectrum of the transfer function can be obtained in advance, the signal distortion caused by the existence of the transmission path can be suppressed and the effectiveness of the fault feature extraction can be improved.

Based on the above theory, as the real bearing fault signal is very complex, the harmonic components and periodic impact components must be removed in advance to approximate the white noise condition, to improve the analysis accuracy. Then the improved trend-line-based transmission path influence eliminated technique can be realized according to the following steps.

(1)   The Fourier transform is applied to the original bearing fault signal to acquire the amplitude spectrum and the phase spectrum. The harmonic and periodic impact components are suppressed using the spectrum editing technique.

(2)   The trend line is extracted using the S–G filtering, and then the influence of complex transmission path is eliminated.

(3)   The results in (2) are edited to suppress the influence of harmonic components. With the help of original phase spectrum and the inverse Fourier transform, the signal which eliminates the influence of transmission path is obtained.

## Optimal Analysis Frequency Band Selection

To select the optimal analysis frequency band, the bandwidth and the central frequency should be proper determined. To extract the fault signatures of REB effectively, the bandwidth should be selected at least three times the fault characteristic frequency. To further highlight the analysis results, in this paper, the bandwidth is set as four times the fault characteristic frequency of REB to ensure the analysis results, and finally only the first three orders of the fault features are exhibited.

Since the theoretical value of fault characteristic frequency for REB may be a fractional number, the bandwidth of the analysis frequency is determined as ceil (4*fault characteristic frequency) in this paper; ceil represents round the number to the nearest integer greater than or equal to that number. The interval of adjacent analysis frequency bands' center frequencies is 100 Hz, and the whole signal is divided. Assuming that the central frequency of the first band is 500, the central frequency of the second band will be 600, and so on. The optimal analysis frequency band is selected in the range from 1 to fs/2, where fs denotes the sampling frequency of the signal.

An appropriate index must be determined to select the optimal analysis band, as the fault features of the REB will exist as the fault characteristic frequency and its harmonics in the envelope spectrum; the maximum energy ratio of fault feature components is used to select the optimal frequency band. For the discrete time signal $x(n)$, its envelope spectrum is $S(n)$ and the energy ratio (ER) of fault feature components can be expressed as:

$$ER = \frac{1}{K} \cdot \frac{\sum_{i=1}^{K} \max[S(f_c \cdot i - 0.02f_c : f_c \cdot i + 0.02f_c)]}{\sum_{i=1}^{fs/2} S(i)} \qquad \text{(Eq 5)}$$

As the speed fluctuations and manufacturing errors are exist in the REB, which make it impossible for the actual fault characteristic frequency to be the same as the theoretical value, the phenomena are taken into consideration, and the feature is determined in the range from 0.98 to 1.02 times the fault characteristic frequency. K denotes the order of the fault characteristic frequency, which is determined as 3 to be consistent with the bandwidth of analysis frequency band, and the significance of the first three orders of fault characteristic frequencies is examined.

## Cross-Correlation Analysis

Due to the existence of original noise, the selection of a single analysis band can easily lead to a lack of fault feature components and the existence of a certain amount of

1168

J Fail. Anal. and Preven. (2022) 22:1164–1179

irrelevant interference. To address this problem, the optimal and suboptimal band signals are both selected, and the cross-correlation analysis is introduced. As the cross-correlation analysis can enhance the same frequency components in the two signals and suppress the irrelevant components, the fault features can be successfully extracted, and the random noise is suppressed.

Supposing $x1(n)$ and $x2(n)$ are the optimal and suboptimal frequency band signal, respectively, the cross-correlation analysis between these two signals can be expressed as:

$$R_{x_1x_2}(m) = \begin{cases} \frac{1}{L}\sum_{n=0}^{L-m-1} x_1(n+m)\tilde{x}_2(n) & m \geq 0 \\ \tilde{R}_{x_1x_2}(-m) & m < 0 \end{cases} \quad \text{(Eq 6)}$$

where $\tilde{x}_2(n)$ represents the conjugate of the signal $x_2(n)$.

## The Whole Structure of the Proposed Method

On basis of the theories described in "Spectrum editing" section to solve the problem of signal distortion and strong interference components caused by complex transmission path and multi-vibration sources in the equipment, a fault feature extraction method based on multiband signals cross-correlation spectrum is proposed, which is then applied to the fault diagnosis of REB under complex transmission path. The flowchart of this technique is depicted in Fig. 1. The detailed steps are described below.

*Step one* The vibration signal of REB is obtained.
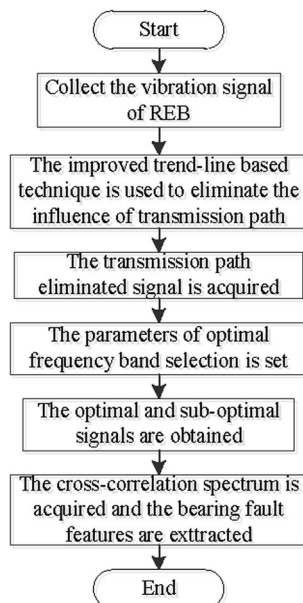


**Fig. 1** Flow chart of the proposed method

*Step two* The influence of complex transmission path is eliminated using the improved trend-line-based technique.

*Step three* The parameters of optimal frequency band selection are set, the whole frequency band is divided, and the ER values of each sub-signals are calculated.

*Step four* The optimal and suboptimal signals determined with the maximum energy ratio of feature components are adopted as the target.

*Step five* The cross-correlation analysis is performed between the two signals acquired in step four; then the Fourier transform is employed to obtain the cross-correlation spectrum where the bearing fault features can be clearly distinguished, and the fault type of REB can also be determined correctly.

## Simulated Verification

The simulation signal is first employed to verify the effectiveness of the proposed method. The construction of simulation signal simulates the existence of bearing inner race defect, which contains the periodic impacts, the frequency modulation, the harmonic components, the noise and so on. The influence of the transmission path is emphasized (represent as the transfer function in the vibration system). The periodic impacts s(t) are simulated by the triangular wave function in MATLAB, and the frequency for impacts is 182 Hz, which means the fault characteristic frequency for the simulation signal is 182 Hz. The simulation signal is expressed as:

$$\begin{cases} y(t) = x(t) * h(t) \\ x(t) = A_i s(t) + B(t) + n(t) \\ A_i = 0.8\cos(2\pi f_r t + \pi/2) + 0.5 \\ B(t) = 0.3\sin(1600\pi t + \pi/6) + 0.2\sin(1040\pi t) \end{cases} \quad \text{(Eq 7)}$$

where $x(t)$ and $y(t)$ denote the excitation signal and the response signal, respectively. $f_r$=42 Hz denotes the rotating speed, $A_i$ denotes the amplitude modulation component with a frequency of $1/f_r$. $B(t)$ denotes the harmonic components which consists of two sine waves. $n(t)$ is the random noise simulated by the randn function in MATLAB. $h(t)$ is the unit pulse response of the transfer function, which can be expressed as:

$$H(s) = \frac{(5000\pi)^2}{s^2 + 4655s + (5000\pi)^2} + \frac{(2500\pi)^2}{s^2 + 1985s + (2500\pi)^2} \quad \text{(Eq 8)}$$

The amplitude spectrum of the transfer function is exhibited in Fig. 2. The sampling frequency of all signals

used in simulation is 32768Hz, and the simulation signal is depicted in Fig. 3. To present the signal more clearly, only 0.1s of the signal is displayed. Due to the interference of harmonics and noise, the periodic impact components cannot be detected both in excitation and response signals. The amplitude of the response signal is generally larger than that of the excitation signal by comparison. In the amplitude spectrum of these two signals, the amplitude of spectral lines 520 and 800 Hz are prominent which corresponds to the harmonic components. What is more, the response signal is significantly distorted due to the influence of the transmission path with the interference components further accentuated. A comparison between Figs. 2 and 3d reveals that the amplitude of the white noise (at the bottom of Fig. 3d) reflects the trend of the transfer function and can be used to suppress the influence of the transmission path. Then, the proposed technique is applied to the simulation signal.

To extract the trend line effectively, the harmonic and periodic impact components in Fig. 3d are suppressed in advance and the result is exhibited in Fig. 4a, where the trend can be obviously observed. Based on the edited amplitude spectrum, the S–G filtering is employed (the window length is determined as 451 based on many trails) and the extracted trend line is shown in Fig. 4b. It can be observed that the trend line is like the trend in the edited amplitude spectrum. The trend line in the amplitude spectrum of the response signal is then removed and the transmission path influence eliminated amplitude spectrum is exhibited in Fig. 4c, where no obvious trend components can be detected in the amplitude of white noise. All features in Fig. 4c are like those in Fig. 3b, which indicates that the influence caused by the transmission path is almost eliminated. Subsequently, the harmonic components in Fig. 4c should be edited and result is depicted in Fig. 4d.

The amplitude spectrum in Fig. 4d is then combined with the phase spectrum of the original response signal; with the help of inverse Fourier transform, the transmission path eliminated signal is obtained which is displayed in Fig. 5. The envelope spectrum is obtained by the Hilbert transform and fast Fourier transform directly. According to
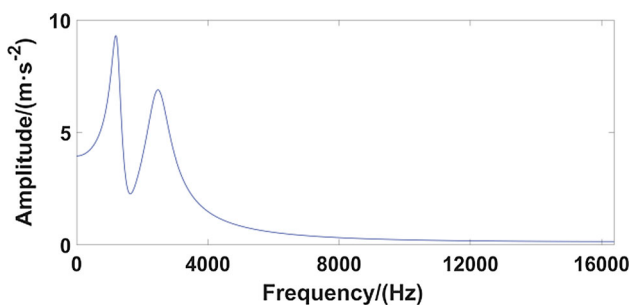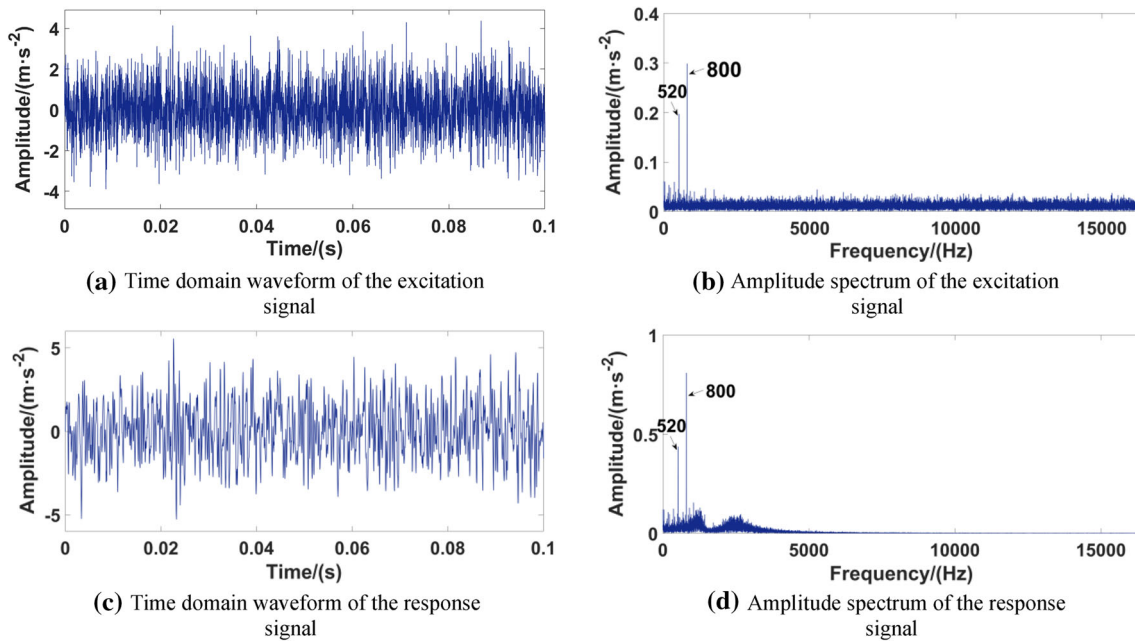
Fig. 5, as the excitation signal also contains strong interference components, no obvious fault features can be identified from either the time domain waveform or the envelope spectrum, and the periodic impact components are unable to be observed. As a result, further process of the signal is required.
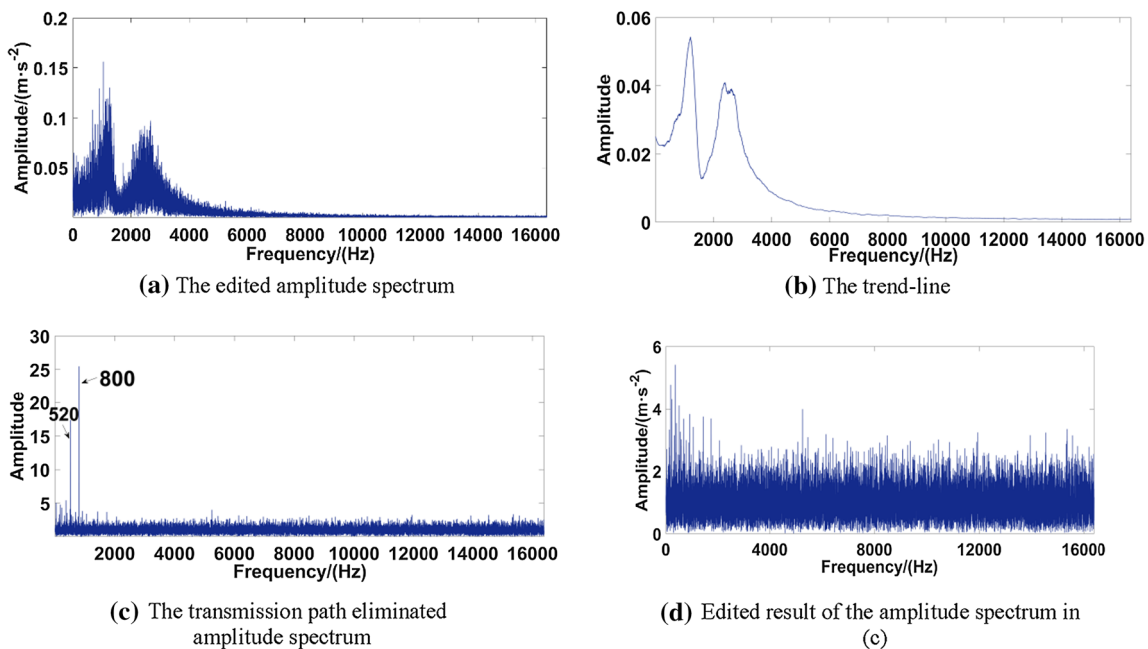
Subsequently, the optimal band selection method is employed. The bandwidth of the frequency band is selected as $182 \times 4 = 728$ Hz. The ER valves of different bands are calculated and the relationship between the frequency bands and ER values is displayed in Fig. 6a. Based on the curve, the maximum ER achieved with the central frequency is 964 Hz, which is determined as the optimal frequency band. Besides, the central frequency of the suboptimal band is determined as 864 Hz. Then the band-pass filters are applied to the transmission path eliminated signal and the optimal band signal and the suboptimal band signal are acquired, which are shown in Fig. 6b and c. Cross-correlation analysis is applied to the two signals; combined with the Fourier transform, the cross-correlation spectrum shown in Fig. 6d is obtained, where the rotating frequency, the fault characteristic frequency and its harmonics are obviously detected. In addition, the side-bands around the fault characteristic frequency components modulated by rotating frequency are also successfully extracted. Based on the above features, it can be concluded that the bearing has inner race defect, which verifies the effectiveness of the proposed technique in bearing fault feature extraction under complex transmission path.

To highlight the effectiveness of the proposed algorithm, the classic Fast kurtogram method is directly applied to the simulation signal and the optimal analysis frequency band is selected; results are exhibited in Fig. 7. Based on the kurtogram in Fig. 7a, the central frequency and bandwidth are determined as 4096 and 8192 Hz, respectively. The corresponding square envelope spectrum of the optimal band signal is exhibited in Fig. 7b, where no fault information is extracted, and the fault type of the REB cannot be judged. The analyzed results reveal that the Fast kurtogram method can hardly extract the weak fault features due to the heavy interference components caused by the complex transmission path.

In addition, as the influence of transmission path is taken into consideration in CYCBD technique which can achieve good results in bearing fault diagnosis, this technique is utilized for further analysis. The value of the cyclic frequency in CYCBD is set based on the characteristic frequency of the target fault type. The length of filter should not be short than the number of signal points contained in one fault cycle; hence, to be consistent with the subsequent experimental analysis, the filter length is chosen as $L = 200$ in this simulation; the analyzed results are shown in Fig. 8. No obvious fault features are successfully



Fig. 2 Amplitude spectrum of the transfer function

1170

J Fail. Anal. and Preven. (2022) 22:1164–1179



(a) Time domain waveform of the excitation signal

(b) Amplitude spectrum of the excitation signal

(c) Time domain waveform of the response signal

(d) Amplitude spectrum of the response signal

Fig. 3 The simulation signal



(a) The edited amplitude spectrum

(b) The trend-line

(c) The transmission path eliminated amplitude spectrum

(d) Edited result of the amplitude spectrum in (c)

Fig. 4 The transmission path eliminated results

extracted both in the deconvolution signal and its envelope spectrum which may result from the inappropriate selection of the filter length. However, the optimal selection of filter length is very time-consuming, which will cost a lot of time. This comparison results further demonstrate the importance, high efficiency and effectiveness of the proposed method in transmission path elimination.

## Experimental Signal Verification

To further demonstrate the effectiveness of the proposed method in fault diagnosis of REB under complex transmission path, the bearing fault signals collected using the test rig in the laboratory are employed. The structure of the test rig is depicted in Fig. 9, which consists the lubrication system, the axial and radial loading system, the main shaft
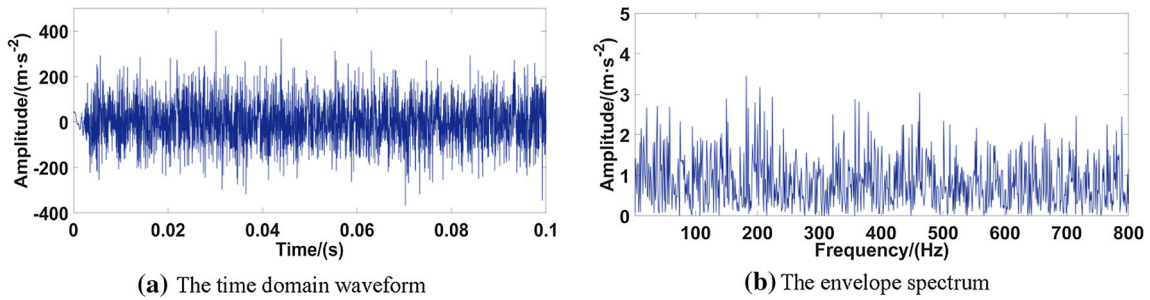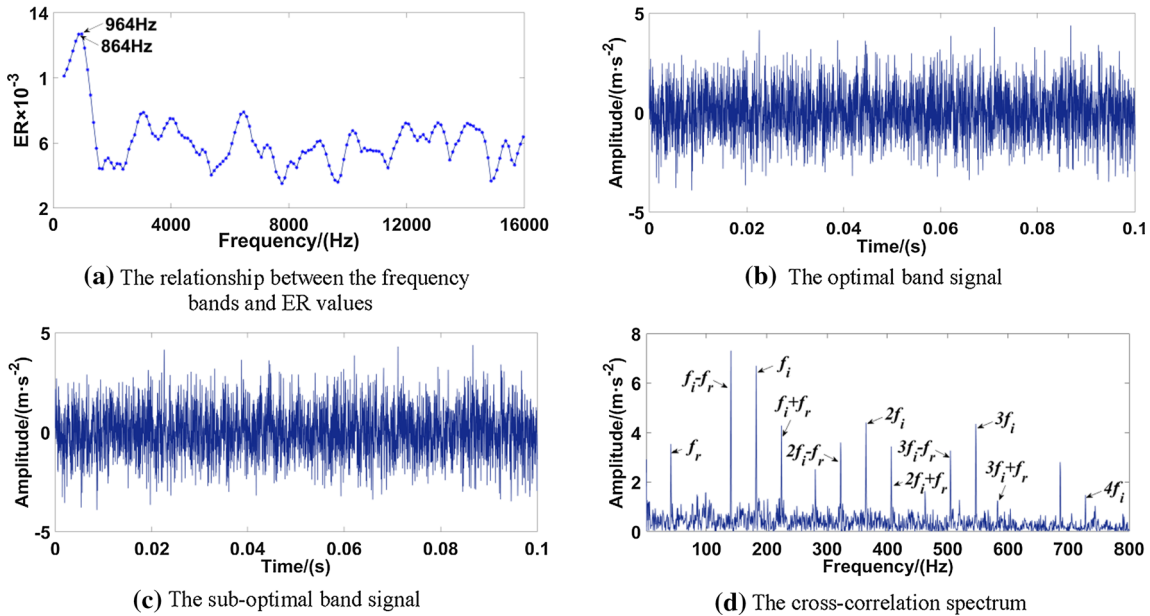
J Fail. Anal. and Preven. (2022) 22:1164–1179

1171



**(a)** The time domain waveform

**(b)** The envelope spectrum

**Fig. 5** The transmission path eliminated signal



**(a)** The relationship between the frequency bands and ER values

**(b)** The optimal band signal

**(c)** The sub-optimal band signal

**(d)** The cross-correlation spectrum

**Fig. 6** Analyzed results of the simulation signal using the proposed method



**(a)** The kurtogram

**(b)** The square envelope signal of the optimal band signal
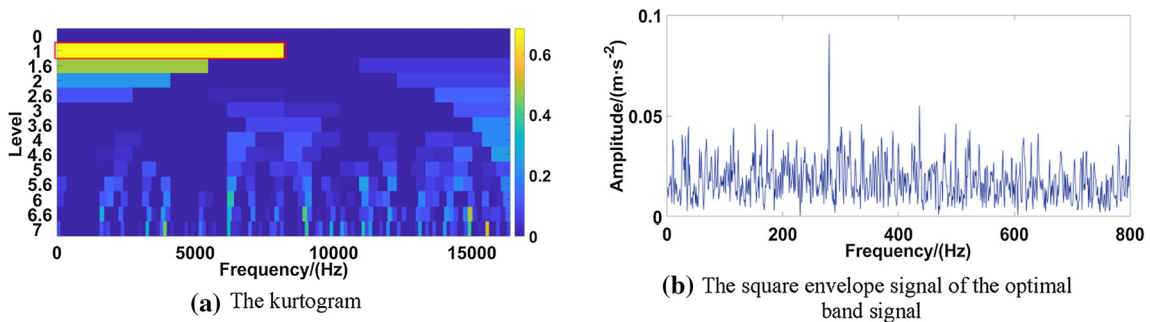
**Fig. 7** Analyzed results of the simulation signal using the Fast kurtogram

and so on. The rotating speed and the load of the test rig can be changed using the control system. Hence, the common working conditions and fault types of REB can be simulated. In this test, to simulate the condition of complex transmission path, the measuring points are selected far from the test bearing (outside of the support structure), which makes the signals may transmit through multiple bolt connection interfaces and affected by the complex structures (multi-vibration sources) of the test rig itself. As a result, the measured bearing vibration signals may be very complex.
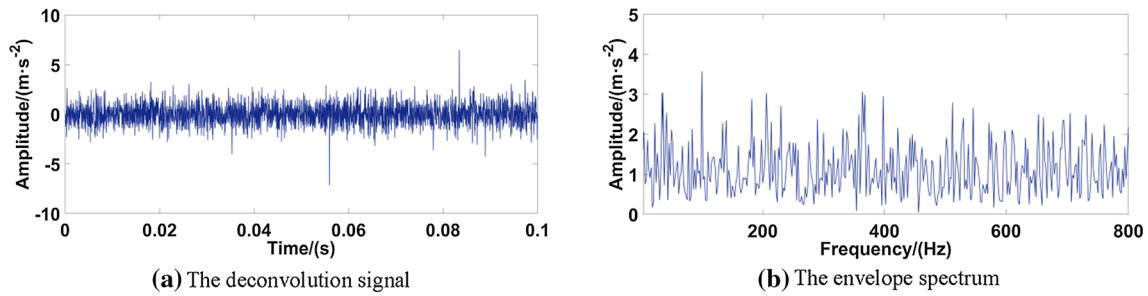
1172

J Fail. Anal. and Preven. (2022) 22:1164–1179



**(a)** The deconvolution signal



**(b)** The envelope spectrum

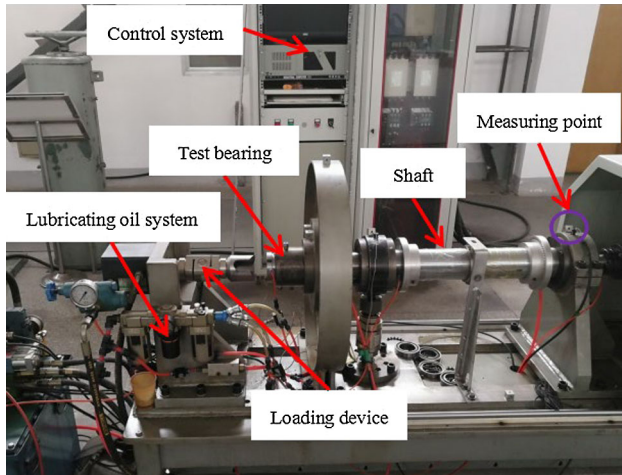**Fig. 8** Analyzed results of the simulation signal using the CYCBD



**Fig. 9** The test rig

**Table 1** Parameters of the test bearing

| Inner diameter (mm) | Outer diameter (mm) | Pitch diameter D (mm) | Ball diameter d (mm) | Number of ball Z | Contact angle α (°) |
|---|---|---|---|---|---|
| 50 | 80 | 65 | 9 | 13 | 0 |

The experimental bearing type is 6010 whose parameters are presented in Table 1. To simulate the existence of inner race and outer race fault, the laser wire-electrode cutting is employed, and a defect is generated (the width and depth of the defect are both 0.2 mm). During the test, the rotating speed is set as 3000r/min($f_r$ = 50 Hz)and the sampling frequency is 32768 Hz; the radial and axial loads are 1KN and 2KN, respectively. The fault characteristic frequency of inner ($f_i$) and outer ($f_o$) race defect can be expressed as:

$$\begin{cases} f_i = \frac{1}{2}Z\left(1 + \frac{d}{D}\cos a\right)f_r \\ f_o = \frac{1}{2}Z\left(1 - \frac{d}{D}\cos a\right)f_r \end{cases} \quad \text{(Eq 9)}$$

By calculation, the theoretical fault characteristic frequency for this REB with inner race and outer race defect is $f_i$ = 370 and $f_o$ = 280Hz.

## REB with Inner Race Defect

The experimental bearing inner race fault signal is exhibited in Fig. 10. Due to the influence of complex transmission path and the multistructures of the test rig, the periodic impacts caused by bearing fault cannot be detected in the time domain signal, and the interference components are obvious. Its envelope spectrum in Fig. 10b shows a complicated feature map with many irrelevant frequency components, only one of the rotating frequency components and the fault characteristic frequency $f_i$ are observed, the extracted fault features are not abundant enough, and the bearing working condition cannot be accurately judged. Therefore, the method in this paper is applied to the signal.

Figure 11a is the amplitude spectrum of the inner race defect signal which displays a complex feature map with numerous spectral lines. However, at the bottom of the figure, the amplitude spectrum of the white noise can also reflect the fluctuation trend, which can be employed to simulate the characteristics of the transmission path. To extract the trend line accurately, the amplitude spectrum is first edited, and the result is exhibited in Fig. 11b, where the interference components in low-frequency part are obviously eliminated. The trend line is then extracted using the S–G filter shown in Fig. 11c. The trend line is combined with the original amplitude spectrum of the signal in Fig. 11a, and the transmission path eliminated amplitude spectrum is acquired in Fig. 11d. It can be observed that the fluctuation trend of white noise at the bottom is significantly eliminated. To further eliminate the influence of irrelevant components, the obvious discrete spectral lines at the rotating frequency components are edited, which may be due to the imbalance and misalignment of the rotating machinery, and the edited result is shown in Fig. 11e.

The edited amplitude spectrum is then combined with the original phase spectrum and the inverse Fourier transform, the signal is changed from frequency domain to the time domain, and the transmission path eliminated inner race fault signal is exhibited in Fig. 12a. The impact components can be detected in this signal. According to the envelope spectrum shown in Fig. 12b, the rotating
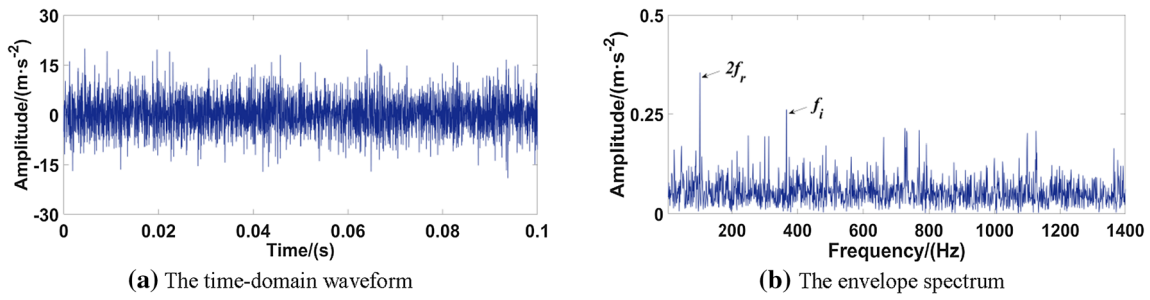
(a) The time-domain waveform

(b) The envelope spectrum

Fig. 10 The experimental bearing inner race fault signal



(a) The amplitude spectrum of the measured signal

(b) The edited amplitude spectrum

(c) The trend-line

(d) The transmission path eliminated amplitude spectrum

(e) The edited result of the amplitude spectrum in (d)
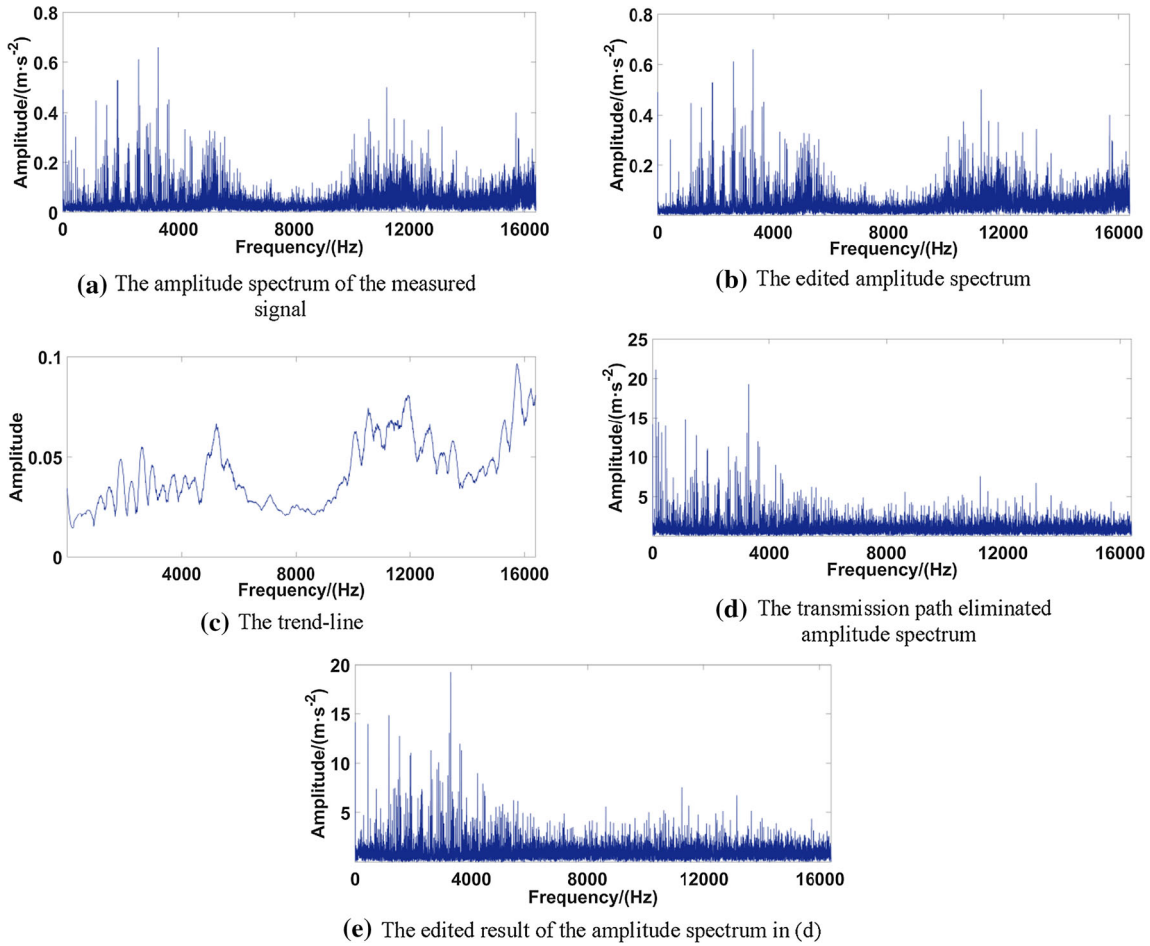
Fig. 11 The transmission path eliminated results of inner race fault signal



(a) The time-domain waveform

(b) The envelope spectrum

Fig. 12 The transmission path eliminated inner race fault signal

1174

J Fail. Anal. and Preven. (2022) 22:1164–1179
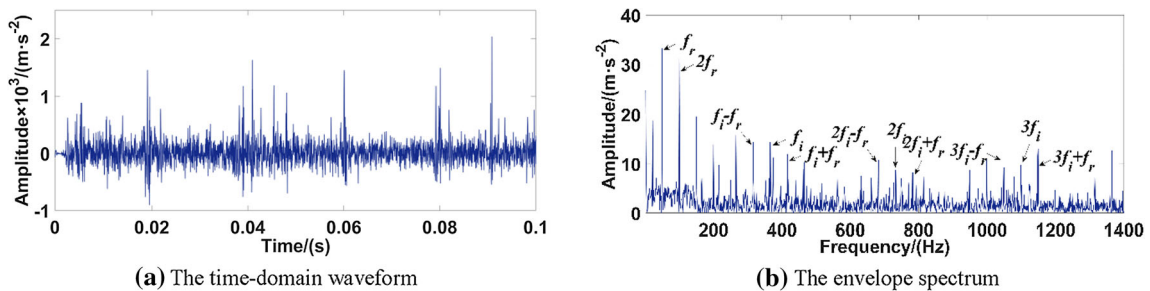
frequency $f_r$ and its harmonic, the fault characteristic frequency $f_i$ and its harmonics, the side-bands around the fault characteristic frequency components modulated by rotating frequency are all observed. The extracted defect signatures are abundant, which demonstrate the essential of transmission path elimination. However, some spectral lines corresponding to fault features are not very prominent, and many interference frequency components can be identified in the whole spectrum. As a result, the signal is further analyzed, and the results are depicted in Fig. 13.

When selecting the optimal analysis frequency band, the bandwidth is determined as $370 \times 4 = 1480$ Hz, Fig. 13a shows the curve of different band signals and their ER values, and the location of the analysis frequency bands is determined. The central frequency of the optimal analysis frequency band is 2140 Hz (the ER value is 0.01027), and the central frequency of the suboptimal analysis frequency band is 2040 Hz (the ER value is 0.0102). The optimal and suboptimal filtered signals obtained using band-pass filtering are exhibited in Fig. 13b and c, respectively. To make full use of the fault features contained in the above two signals, the cross-correlation analysis is utilized, and the influence of interference components is further suppressed. The cross-correlation spectrum in Fig. 13d shows abundant bearing fault features, where the rotating frequency components, the fault characteristic frequency components and their side-bands are all clearly detected. Compared with the results in Fig. 12b, the amplitude of the spectral lines at the characteristic frequency is more prominent using the proposed technique. What is more, the suppression effect of irrelevant noise is more obvious,
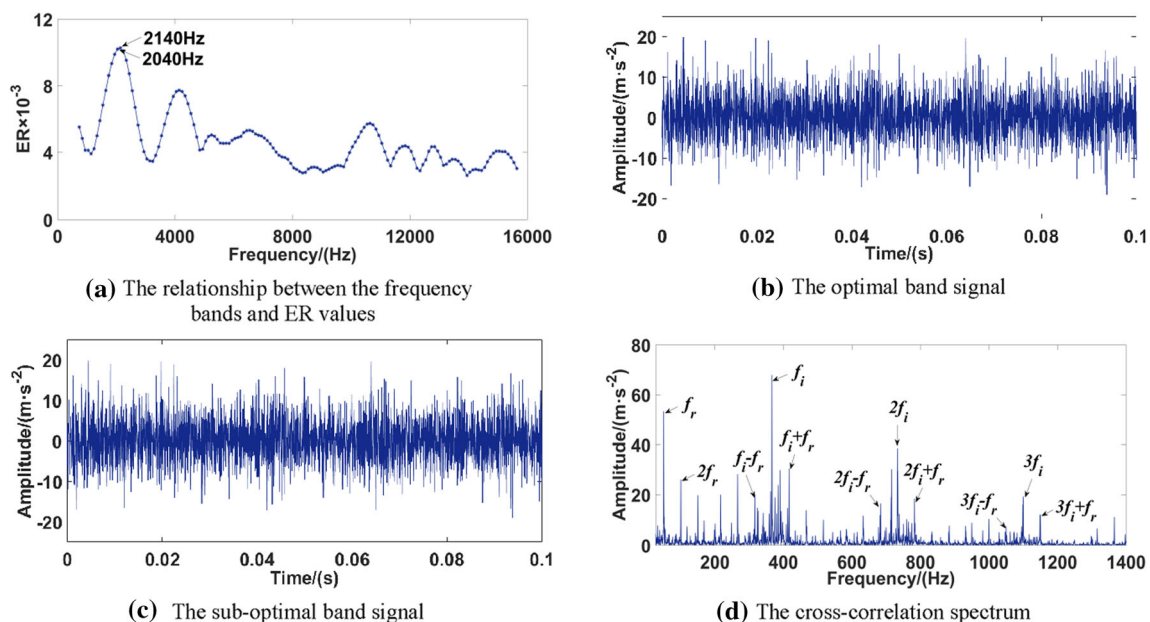
which demonstrate the effectiveness of the proposed technique.

Analogously, two comparison methods are still used to process the measured bearing inner race fault signals. First, the analyzed results using the Fast kurtogram are exhibited in Fig. 14. According to the kurtogram in Fig. 14a, the central frequency and bandwidth of the optimal frequency band can be determined as 15018 and 2730 Hz, and the square envelope spectrum of the optimal band signal is displayed in Fig. 14b. Only the spectral line at 100 Hz is obvious which is one of the rotating speed components, and the fault signatures are unable to be detected, which draws a conclusion that the signal distortion and interference components caused by the complex transmission path led to the failure of the Fast kurtogram method.

Subsequently, the CYCBD technique is applied to the experimental signal, the filter length is selected as 200, and the results are shown in Fig. 15. As in Fig. 15a, although the interference components are attenuated, the impact components caused by the bearing defect are still not obvious. Its envelope spectrum is heavily influenced, the bearing inner race fault characteristic frequency fi and one of its harmonics can hardly observed, and the fault features are not abundant enough to identify the bearing fault correctly.

## REB with Outer Race Defect

To show the applicable of the proposed technique, the experimental bearing outer race defect signal is employed.



**(a)** The relationship between the frequency bands and ER values

**(b)** The optimal band signal

**(c)** The sub-optimal band signal

**(d)** The cross-correlation spectrum

**Fig. 13** Analyzed results of the inner race fault signal using the proposed method

**(a)** The kurtogram

**(b)** The square envelope signal of the optimal band signal

**Fig. 14** Analyzed results of the inner race fault signal using the Fast kurtogram



**(a)** The deconvolution signal
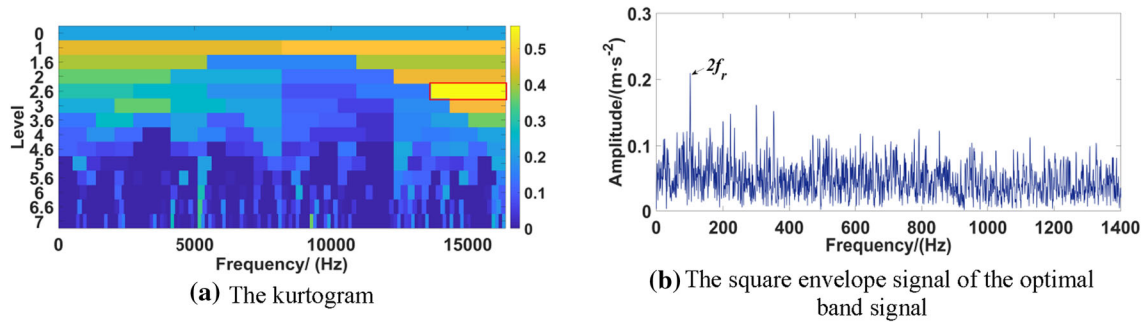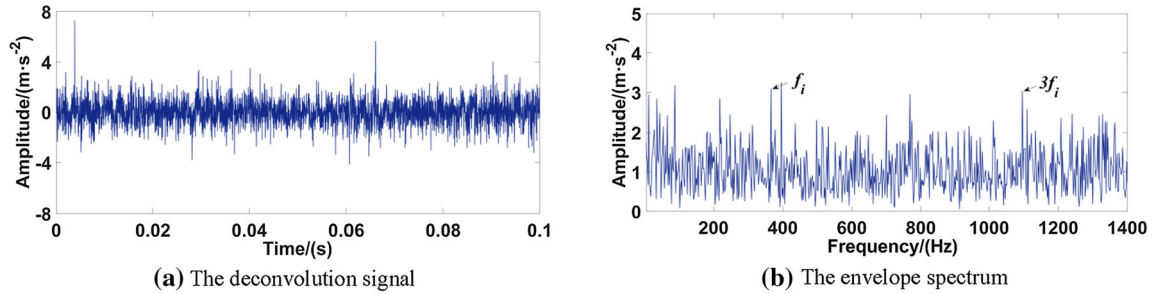
**(b)** The envelope spectrum

**Fig. 15** Analyzed results of the inner race fault signal using the CYCBD

The time domain waveform and envelope spectrum of the signal are shown in Fig. 16. The periodic impacts cannot be observed in Fig. 16a due to the influence of complex structure of the equipment and the transmission path. The frequency components in Fig. 16b are very complex, and no valid defect information can be reflected. Hence, the direct use of envelope analysis cannot achieve the ideal results and the method in this paper is employed.

The amplitude spectrum of the measured signal calculated by the FFT is shown in Fig. 17a, which is very complex with no useful information to be observed. But the amplitude spectrum of the white noise at the bottom can still reflect the trend of signal distortion caused by the complex transmission path. Hence, the influence of transmission path can also be eliminated by extracting this trend line. The amplitude spectrum is edited to suppress the spectral lines at the periodic and harmonic frequencies to

ensure the accuracy of trend-line calculation. The edited result in Fig. 17b exhibits that the discrete spectral lines in the low-frequency part are significantly suppressed. Figure 17c shows the trend line extracted using the S–G filtering, and the window length is chosen as 45, which shows the similar trend with the amplitude spectrum in Fig. 17b, and no significant distortion appears. The influence of complex transmission path is eliminated based on the extracted trend line shown in Fig. 17d. Moreover, Fig. 17e is the edited result of Fig. 17d. According to the two-amplitude spectrum, it can be found that the trend of white noise's amplitude spectrum is no longer exist, which indicates that the influence of complex transmission path is suppressed effectively.

Subsequently, the edited amplitude spectrum in Fig. 17e, the original phase spectrum and the inverse Fourier transform are combined to acquire the transmission
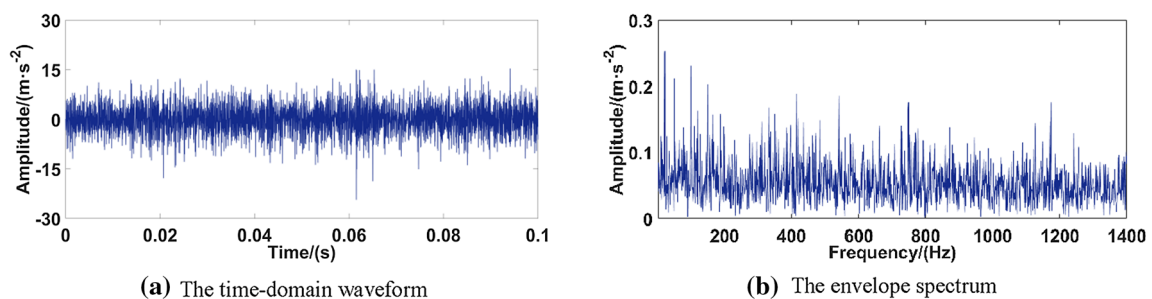


**(a)** The time-domain waveform

**(b)** The envelope spectrum

**Fig. 16** The experimental bearing outer race fault signal

1176

J Fail. Anal. and Preven. (2022) 22:1164–1179



(a) The amplitude spectrum of the measured signal

(b) The edited amplitude spectrum

(c) The trend-line

(d) The transmission path eliminated amplitude spectrum

(e) The edited result of the amplitude spectrum in (d)
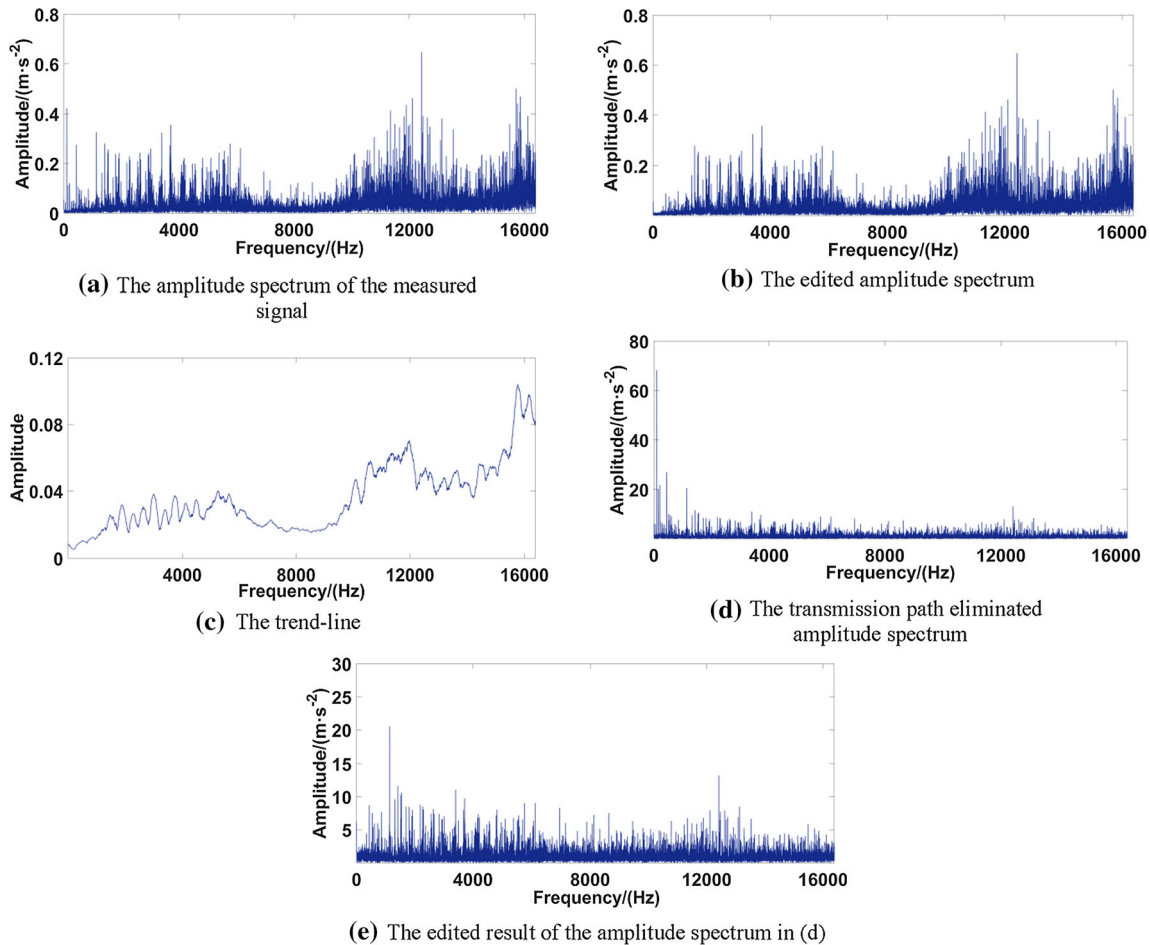
**Fig. 17** The transmission path eliminated results of the outer race fault signal



(a) The time-domain waveform
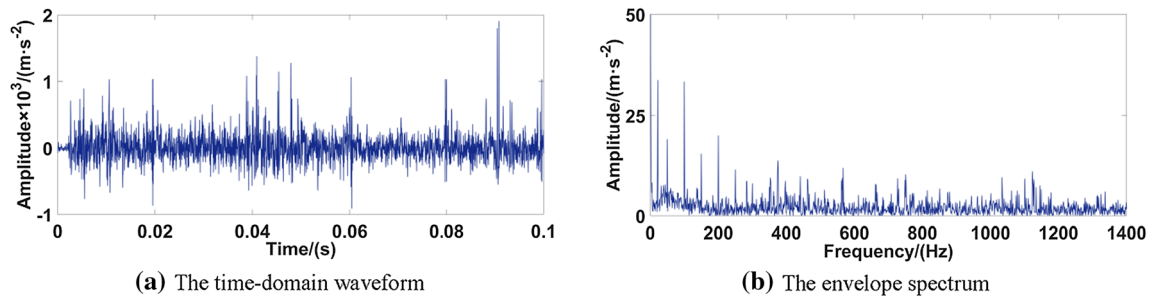
(b) The envelope spectrum

**Fig. 18** The transmission path eliminated outer race fault signal

path eliminated signal. As shown in Fig. 18a, the impact characteristics can be detected, and the interference components are significantly suppressed. Its envelope spectrum is displayed in Fig. 18b where no useful feature components are successfully extracted. Only the rotating frequency and its harmonics can be observed in the low-frequency part which may result from the imbalance of the rotating part. The above phenomena indicate that the transmission path elimination is not enough, and the fault extraction is still difficult when the original noise is very strong. Thus, some other signal processing technique is required.

Figure 19 shows the results using the method in this paper. The bandwidth is determined as $280 \times 4 = 1120$ Hz when selecting the optimal analysis frequency band and the relationship of each analysis frequency bands, and their ER values are shown as the curve in Fig. 19a. According to the figure, the central frequencies of the optimal and suboptimal analysis bands are determined 1460 and 1360 Hz, respectively, and the corresponding ER values are 0.00709
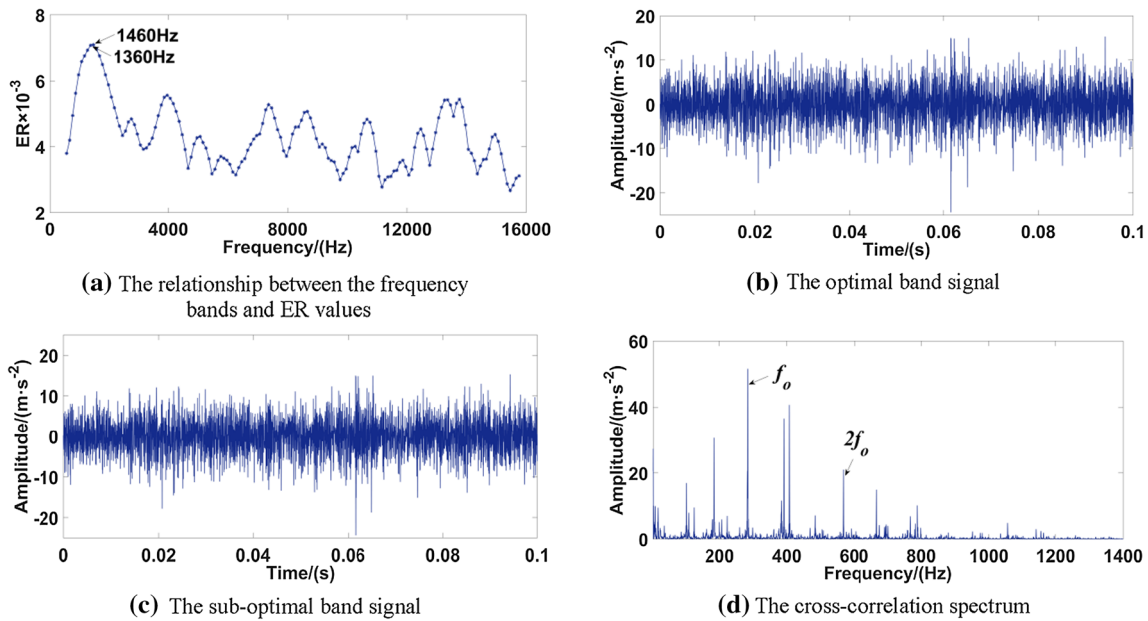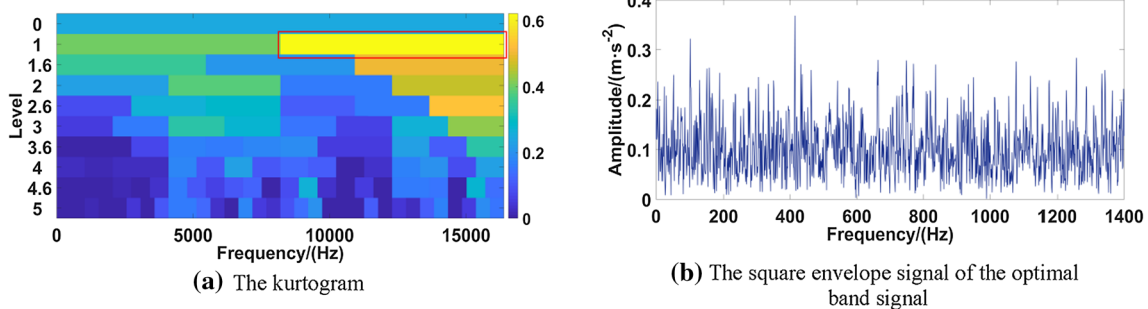
**Fig. 19** Analyzed results of the outer race fault signal using the proposed method

and 0.00707. Then the optimal and suboptimal signals are acquired and exhibited in Fig. 19b and c. The cross-correlation analysis is applied to enhance the fault features in both signals, and with the help of the FFT, the cross-correlation spectrum is acquired shown in Fig. 19d. Based on this figure, the bearing outer race defect frequency $f_o$ and one of the harmonics is clearly observed, which can be used for the determination of bearing fault type. Compared with the result in Fig. 16b, the effectiveness of the algorithm in eliminating the influence of complex transmission paths, suppressing noise components and accurately extracting the weak fault signatures of REB is highlighted.

Similarly, the analyzed results of the measured bearing outer race fault signal using the Fast kurtogram and the CYCBD are exhibited in Figs. 20 and 21. According to Fig. 20, the central frequency and bandwidth of the optimal analysis frequency band are determined as 12288 and 8192

Hz, respectively. But in the square envelope spectrum of the optimal band signal, no useful fault features is extracted due to heavily influence caused by the strong background noise. When the CYCBD technique is employed, the filter length is still set as 200 and the results are presented in Fig. 21. The periodic impact components caused by the bearing fault are not prominent in the deconvolution signal, and the interference component is still evident. The envelope spectrum in Fig. 21b still fails to extract any fault information, which indicates that the influence of transmission path is not solved.

On basis of the two comparisons, it is further demonstrated that the proposed method can suppress the signal distortion and interference components enhancement caused by complex transmission paths, and the effectiveness in extracting fault signatures of REB is guaranteed.



**Fig. 20** Analyzed results of the outer race fault signal using the Fast kurtogram

**(a)** The deconvolution signal　　**(b)** The envelope spectrum
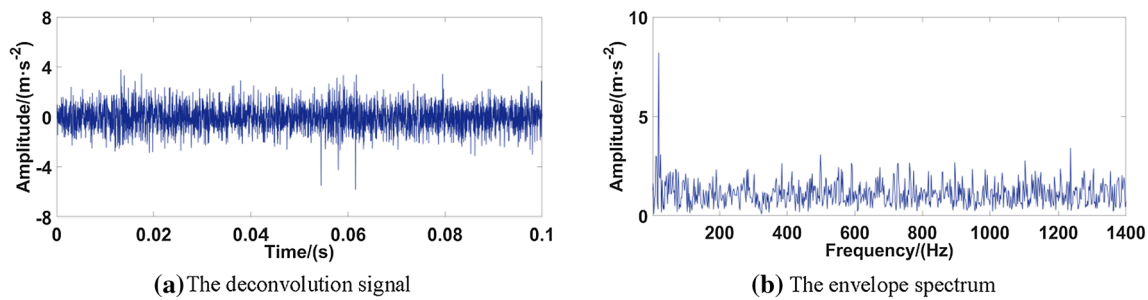
**Fig. 21** Analyzed results of the outer race fault signal using the CYCBD

## Conclusion

To extract the fault features of REB efficiently and accurately under the influence of complex transmission path, a fault diagnosis method of REB based on the multiband signals cross-correlation spectrum is proposed, which has certain practice value. Through the research of this paper, some conclusions are drawn as follows:

(1) The improved transmission path elimination technique is employed to suppress the influence of signal distorted and irrelevant components, which simplifies the calculation process, and the analysis accuracy is ensured.

(2) The multiband signals cross-correlation spectrum technique is employed. This method further suppresses the interference of irrelevant noise by optimal analysis frequency band selection, which avoids the determination of resonance bands by human experience. Multiband signals are utilized to guarantee the abundance of fault features. With the advantage of cross-correlation analysis, the fault signatures of REB are enhanced and extracted successfully.

(3) The existence of complex transmission path is simulated in simulation and experimental analysis, and the effectiveness of the proposed technique is demonstrated. Results indicate that this method can extract the fault signatures of REB under the influence of complex transmission path while the accurate determination of bearing fault type is realized.

## References

1. J. Antoni, Fast computation of the kurtogram for the detection of transient faults. Mech. Syst. Signal Process. **21**(1), 108–124 (2007)
2. Z. Liu, S. Yang, Y. Liu et al., Adaptive correlated Kurtogram and its applications in wheelset-bearing system fault diagnosis. Mech. Syst. Signal Process. **154**, 107511 (2021)
3. K. Zhang, Y. Xu, Z. Liao et al., A novel Fast Entrogram and its applications in rolling bearing fault diagnosis. Mech. Syst. Signal Process. **154**, 107582 (2021)
4. Y. Xu, Y. Deng, C. Ma et al., The Enfigram: a robust method for extracting repetitive transients in rolling bearing fault diagnosis. Mech. Syst. Signal Process. **158**, 107779 (2021)
5. L. Wang, Z. Liu, H. Cao et al., Subband averaging kurtogram with dual-tree complex wavelet packet transform for rotating machinery fault diagnosis. Mech. Syst. Signal Process. **142**, 106755 (2020)
6. K. Zhang, P. Chen, M. Yang et al., The Harmogram: a periodic impulses detection method and its application in bearing fault diagnosis. Mech. Syst. Signal Process. **165**, 108374 (2022)
7. Q. Liu, J. Yang, K. Zhang, An improved empirical wavelet transform and sensitive components selecting method for bearing fault. Measurement. **187**, 110348 (2021)
8. K. Yu, T.R. Lin, J. Tan et al., An adaptive sensitive frequency band selection method for empirical wavelet transform and its application in bearing fault diagnosis. Measurement. **134**, 375–384 (2019)
9. Y. Xu, Y. Cai et al., An enhanced bearing fault diagnosis method based on TVF-EMD and a high-order energy operator. Measure. Sci. Technol. (2018). https://doi.org/10.1088/1361-6501/aad499
10. J. Chen, L. Cheng, H. Yu et al., Rolling bearing fault diagnosis and health assessment using EEMD and the adjustment Mahalanobis-Taguchi system. Int. J. Syst. Sci. **49**(1), 147–159 (2018)
11. J. Gu, Y. Peng, An improved complementary ensemble empirical mode decomposition method and its application in rolling bearing fault diagnosis. Digital Signal Process. **113**, 103050 (2021)
12. T. Han, Q. Liu, L. Zhang et al., Fault feature extraction of low speed roller bearing based on Teager energy operator and CEEMD. Measurement. **138**, 400–408 (2019)
13. J. Yuan, F. Ji, Y. Gao et al., Integrated ensemble noise-reconstructed empirical mode decomposition for mechanical fault detection. Mech. Syst. Signal Process. **104**, 323–346 (2018)
14. D. Wang, Y. Cai, L. Kwok et al., Making EEMD more effective in extracting bearing fault features for intelligent bearing fault diagnosis by using blind fault component separation. J. Intell. Fuzzy Syst. Appl. Eng. Technol. **34**(6), 3429–3441 (2018)
15. X. Jiang, J. Wang, J. Shi et al., A coarse-to-fine decomposing strategy of VMD for extraction of weak repetitive transients in fault diagnosis of rotating machines. Mech. Syst. Signal Process. **116**, 668–692 (2019)
16. H. Li, Y. Xu, D. An et al., Application of a flat variational modal decomposition algorithm in fault diagnosis of rolling bearings. J. Low Frequency Noise Vib. Active Control. **39**(2), 335–351 (2020)
17. R. Gu, J. Chen, R. Hong et al., Incipient fault diagnosis of rolling bearings based on adaptive variational mode decomposition and Teager energy operator. Measurement. **149**, 106941 (2020)

J Fail. Anal. and Preven. (2022) 22:1164–1179

1179

18. D. Zhu, G. Liu, W. He et al., Fault feature extraction of rolling element bearing based on EVMD. J. Braz. Soc. Mech. Sci. Eng. **43**(12), 1–14 (2021)

19. Y. Miao, M. Zhao, J. Lin, Identification of mechanical compound-fault based on the improved parameter-adaptive variational mode decomposition. ISA Trans. **84**, 82–95 (2019)

20. L. Wang, Z. Liu, Q. Miao et al., Complete ensemble local mean decomposition with adaptive noise and its application to fault diagnosis for rolling bearings. Mech. Syst. Signal Process. **106**, 24–39 (2018)

21. H. Li, T. Liu, X. Wu et al., A bearing fault diagnosis method based on enhanced singular value decomposition. IEEE Trans. Industr. Inf. **17**(5), 3220–3230 (2020)

22. B. Pang, G. Tang, Y. He et al., Weak fault diagnosis of rolling bearings based on singular spectrum decomposition, optimal Lucy-Richardson deconvolution and speed transform. Meas. Sci. Technol. **31**(1), 015008 (2019)

23. Y. Gao, M. Karimi, A.A. Kudreyko et al., Spare optimistic based on improved ADMM and the minimum entropy de-convolution for the early weak fault diagnosis of bearings in marine systems. ISA Trans. **78**, 98–100 (2017)

24. L. Zhang, B. Cai, G. Xiong, et al. Multistage fault feature extraction of consistent optimization for rolling bearings based on correlated kurtosis. Shock Vib. (2020)

25. G.L. McDonald, Q. Zhao, Multipoint optimal minimum entropy deconvolution and convolution fix: application to vibration fault detection. Mech. Syst. Signal Process. **82**, 461–477 (2017)

26. Y. Lab, G. Ca, C. La, Research on bearing fault diagnosis based on spectrum characteristics under strong noise interference. Measurement. **169**, 108509 (2020)

27. M. Buzzoni, J. Antoni, G. D'Elia, Blind deconvolution based on cyclostationarity maximization and its application to fault identification. J. Sound Vib. **432**, 569–601 (2018)

28. B. Zhang, Y. Miao, J. Lin et al., Adaptive maximum second-order cyclostationarity blind deconvolution and its application for locomotive bearing fault diagnosis. Mech. Syst. Signal Process. **158**, 107736 (2021)

29. Z. Wang, J. Zhou, W. Du et al., Bearing fault diagnosis method based on adaptive maximum cyclostationarity blind deconvolution. Mech. Syst. Signal Process. **162**, 108018 (2022)

30. R. Duan, Y. Liao, L. Yang et al., Minimum entropy morphological deconvolution and its application in bearing fault diagnosis. Measurement. **182**, 109649 (2021)

31. Y. Cheng, B. Chen, W. Zhang, Adaptive multipoint optimal minimum entropy deconvolution adjusted and application to fault diagnosis of rolling element bearings. IEEE Sens. J. **19**(24), 12153–12164 (2019)

32. D. Zhu, J. Chen, B. Yin, Fault feature extraction of rolling element bearing based on TPE-EVMD. Measurement. **183**, 109880 (2021)